Collective Organization Behaviors of Multi-Cell Systems Induced by Engineered ECM-Cell Mechanical Coupling

Xiaochen Wang, 1,2,3 Hangyu Li,4,5 Yu Zheng,6,7 Dongshi Guan,4,5 Aidan Wang⁸
Qihui Fan,^{2*} Yang Jiao,6,7* Fangfu Ye^{1,2,3*}

¹Oujiang Laboratory (Zhejiang Lab for Regenerative Medicine, Vision and Brain Health); Wenzhou Institute, University of Chinese Academy of Sciences, Wenzhou, Zhejiang 325000, China;

²Beijing National Laboratory for Condensed Matter Physics, Institute of Physics, Chinese Academy of Sciences, Beijing 100190, China;

³School of Physical Sciences, University of Chinese Academy of Sciences, Beijing 100049, China;

⁴State Key Laboratory of Nonlinear Mechanics, Institute of Mechanics, Chinese Academy of Sciences, Beijing 100190, China;

⁵School of Engineering Science, University of Chinese Academy of Sciences, Beijing 100049, China

⁶Materials Science and Engineering, Arizona State University, Tempe, Arizona, 85287;
⁷Department of Physics, Arizona State University, Tempe, Arizona, 85287⁸Aidi School, Beijing, China.

* Corresponding author: fye@iphy.ac.cn(F.Y.); yang.jiao.2@asu.edu(Y.J.); fanqh@iphy.ac.cn (Q. F.)

Abstract

Mechanical signaling plays a vital role in collective cell behaviors involved in various biological processes. Cells *in vivo* are surrounded by the fibrous extracellular matrix (ECM), which can mediate the propagation of active cellular forces through stressed fiber bundles and regulate the migration of individual cells. However, the mechanisms for multi-cellular organization and collective dynamic induced by cell-ECM mechanical couplings, which are crucial for the development of novel ECM-based biomaterial for cell manipulation and biomechanical applications, remain poorly understood. Here, we elucidate the cell-ECM mechanical coupling mechanisms and the resulting collective organizational behaviors in multi-cellular systems, by designing an *in vitro* quasi-3D experimental system and seeding discrete cell populations on different substrates, enabling the engineering of cell-substrate

coupling. Specifically, we demonstrate a transition between spreading and aggregating in collective organizational behaviors of discrete multi-cellular systems, induced by engineered cell-ECM mechanical coupling by modifying solid substrates to collagen hydrogels, whose mechanisms differ fundamentally from that of cells' monolayer. The collagen-induced intercellular attraction combines to form a centripetal force field, which guides cells' aggregation motions during the aggregation process. During the process of collective cell organization, the collagen substrate undergoes reconstruction into a dense fiber network structure that is correlated with local cellular density and consistent with observed enhanced cells' motility. The weakening of fiber bundle formation within the hydrogel, associated with a low gelation temperature, also reduces cells' movement. Moreover, cells can form different aggregation patterns, responding to the curvature and shape of the original cell population. Our study on ECM-mediated mechanical coupling and collective cell motion regulated by collagen hydrogel provides important insights for fundamental biophysical research, potential new therapies, and tissue engineering applications.

1. Introduction

Collective cell behaviors are fundamental to various biological processes, including tissue formation, wound healing, immune response, and cancer cell invasion^[1-4]. Cells work together to perform specific tasks, such as dividing, migrating, and recognizing, through various communication mechanisms like chemical signals, electrical impulses, and mechanical interactions^[3, 5-8]. In these processes, the ability of cells to sense and respond to mechanical signals is a critical aspect of their functions, playing a vital role in maintaining tissue homeostasis and adapting to environmental changes^[9-15].

In vivo, cells are surrounded by the extracellular matrix (ECM), which provides structural support and transmits mechanical signals^[16, 17]. The ECM can deform, stretch or stiffen due to mechanical forces exerted by the cells, which in turn cause changes in the ECM microstructure that can be sensed by cells through integrins, focal adhesions, and cytoskeletal elements^[18-20]. The ECM, therefore, mediates mechanical signaling between the cells that do not directly contact each other, regulating their collective behaviors and maintaining tissue integrity^[21].

On the other hand, cells can sense mechanical signals and reorganize the ECM to generate mechanical signals. They actively generate tensile or compressive forces to reorganize the ECM, causing fiber alignment, organization, and stiffness changes^[18]. During migration, the auto-myosin network contraction is propagated to the ECM through cells' focal adhesion, causing a deformation of the ECM^[17]. The collagen fibers between adjacent cells can be significantly reorganized and remodeled to form thick fiber bundles that are very effective force carriers, leading to strongly correlated migration of the cells^[19, 22-24]. Recently, the force-guided motion of single cells has been demonstrated, which critically depends on ECM-mediated force transmission^[25-27].

ECM remodeling is critical for many biological processes, such as tissue development, wound healing, and tissue repair^[2, 18]. Despite the recent progress in understanding ECM-mediated force transmission in regulating individual cell dynamics, how the cell-ECM mechanical coupling can give rise to a distinct spectrum of collective dynamics and multi-cellular organizational behaviors is not well understood.

Here, we demonstrate a transition in collective organizational behaviors of multi-cellular systems induced by cell-ECM mechanical coupling. This is achieved by designing an in vitro quasi-3D experimental system and seeding discrete cell populations on different substrates, varying the nature of cell-substrate coupling. By investigating time-lapse images and tracking cells' trajectories, we observed a well-defined spreading-aggregating transition in a simple convex-shaped cell population, when the solid substrate is replaced by the collagen hydrogel. From the collagen deformation field, we find that individual cell contraction forces combine to form a centripetal force field, which guides cell motions during the aggregation process. Interestingly, we also observe a non-trivial dependence of the aggregation behavior on the curvature and shape of the original cell population. For example, in the case of a "Wound pattern" (a concentric ring structure with a hollow center), strong contraction forces transmitted via the fiber bundles between circumferentially adjacent cells led to a collective centripetal migration near the wound boundary.

During collective cell organization, the collagen substrate was reconstructed into a dense fiber network structure, correlated with local cellular density and consistent with observed enhanced cells' motility, providing further evidence for collagen-induced intercellular attraction and resulting collective dynamics. When the fiber bundle formation is weakened within the hydrogel associated with a low gelation temperature, the cell movements also reduce. Moreover, similar behaviors are also observed in different types of cells, indicating that the cell collective motion triggered by collagen-mediated mechanical signaling follows a universal mechanism. By studying ECM-mediated mechanical coupling and collective cell motion regulated by collagen hydrogel, we obtained results that not only contribute to fundamental biophysical research but also have implications for new therapies and tissue engineering. The study provides valuable insights into the importance of mechanical signals in regulating cell behavior, as well as the potential of ECM remodeling in tissue regeneration and engineering.

2. Results

2.1 Collagen Substrate Induces Collective Cell Aggregation

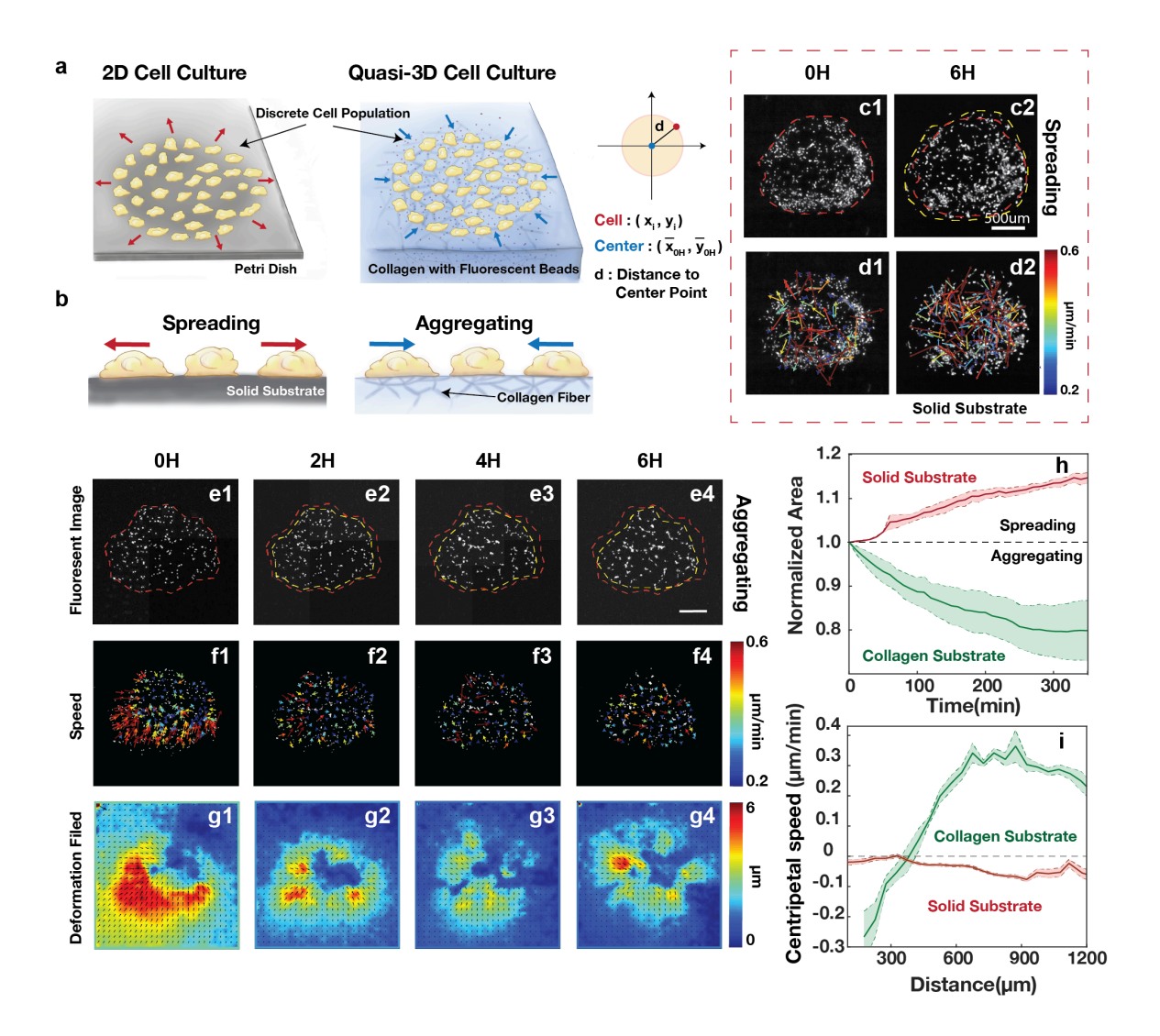


Figure 1 Collagen Substrate Induces Cell Collective aggregation. a-b) Schematic of 2D (left) and quasi-3D (right) in vitro system with discrete cell populations. On the Petri dish, cell population expands outward (c1-c2) with random velocities (d1-d2). On the top of fibrous collagen hydrogel, the cell population retracts and decreases in size. Phase contrast images (e1-e4, red dashed line: cell population boundary at 0H), cells' velocity (f1-f4) and deformation filed with 10mins interval (g1-g4) for a "Round Pattern" cell population with radius 2000 μ m on the collagen substrate. Evolution of cell population size (h) and spatial distribution of the centripetal velocity (i). Data are presented as mean \pm s.e.m. n > 500 data points. Scale bar $= 500 \mu$ m.

We developed an in vitro experimental system to investigate the regulation of the collective behavior of discrete cell populations (i.e., initially non-contacting dispersion of cells) by the extracellular matrix. We aim to regulate cells' collective behaviors by introducing contraction force transmitted through the extracellular matrix. To accomplish this, we seeded discrete cell populations consisting of human mammary gland epithelial cells (MCF10A), each approximately 2000 µm in size, on either the Petri dish or the collagen I hydrogel (Fig.1a).

Compared to a solid substrate, the collagen I hydrogel is a non-linear elastic fibrous material and a standard component in vivo that can generate long-range mechanical signal propagation

by changing the local hardness gradient and microstructure^[9, 18]. We seeded cells on the solid substrate (Petri dish) within a polydimethylsiloxane (PDMS) chamber. One hour after the cells' attachment, we removed the confining chamber, and the cells spread randomly, causing the cell population to expand outward (Fig.1c).

Next, we introduced the 2mg/mL collagen I hydrogel to create a quasi-3D experimental system and deposited the cells directly on the top of the collagen. The cell population started retracting, decreasing in size and eventually forming a dense cell aggregate after 17 hours (Fig. 1e, Fig. S1). This movement changes from spreading to aggregating, referred to as a transition in cells' collective behaviors. In contrast to previous active models that focus on the spreading process of cell monolayers^[28], our quasi-3D experimental system consists of discrete cells without direct force transmission through adhesive junctions. However, the cells can also transmit mechanical signals by deforming the collagen substrate. We know from previous studies that cells can restructure collagen during migration, and the reorganized collagen bundle can carry tensile forces, significantly enhancing intercellular interactions^[25]. When the substrate changed to collagen, the cells' dynamic transitioned from random motion to collective migration (Fig.1i), prompting us to explore the mechanisms underlying this correlated motion.

To measure the collagen deformation field of this quasi-3D experimental system, we mixed fluorescent micro-beads (0.8 um in diameter) in collagen and quantified collagen deformation amplitude fields according to micro-bead displacements by the particle image velocimetry (PIV) analysis technique. As the cell population aggregated, the cells generated radial inward-pointing tractions (Fig.1g). When a single cell is on the collagen surface, it generates a force field centered around the cell through the contraction. The cell population arranged itself in a circular pattern on the collagen surface. The forces from individual cells are coupled together to form a centripetal force field toward the center of the collagen substrate (Fig.1g1). This force field had already existed at the initial moment, and the average speed of cells at the same location was larger than adjacent beads within ECM (Fig. S2), proving that the cell population continued to move under the guidance of the centripetal force field.

We recorded cells' migration using time-lapse inversed microscopy and confocal microscopy at 10 mins intervals for 6 hours. We tracked the trajectories of cells migrating on 2D and quasi-3D substrates and calculated the velocities (Figure 1). The random migration of cells on the solid substrate could be regarded as diffusive during the 6 hours of observation. By contrast, cells seeded on collagen exhibited clear collective migration toward the center of the population. To characterize the spatial distribution of cells' movement, we calculated each cell's location and centripetal velocity relative to the center. A positive centripetal velocity indicates that the cell is moving toward the center, while a negative velocity indicates outward diffusion. We defined the central point as the average coordinates of all cells' positions at the initial time. On a solid surface, the centripetal velocities of cells are negative and do not vary with distance, indicating uniform outward diffusion. However, on the collagen substrate, the average centripetal velocity of cells is larger than 0 and positively correlated with distance. The velocity of cells located more than 900 µm away shows a slight

decrease. Within the range of 350 μ m, the centripetal velocities of cells are negative. Because, as approaching the center, the selection of the center point significantly influences the centripetal velocity direction. During the aggregation process, the center points constantly change, leading to an inaccurate definition of centripetal velocity.

2.2 Boundary Curvature Influences Cells' Organizational Behavior

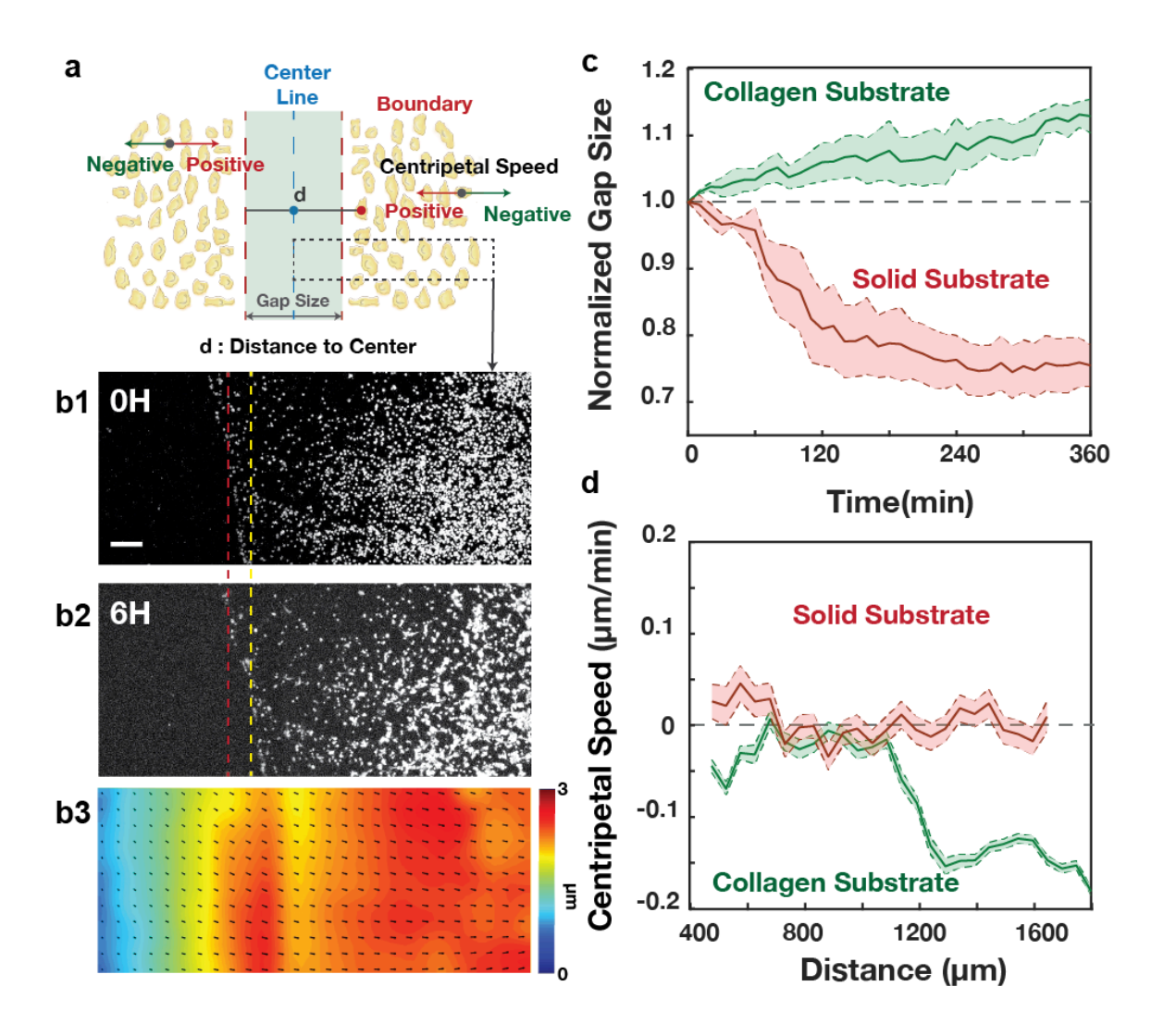


Figure2 Collective aggregation of cell population with straight boundary. a) Illustration of the discrete cell population with a straight boundary. b1-b2) On the top of collagen hydrogel, the cell population aggregates with the boundary right shifting (Red: 0H, Yellow: 6H). b3) Average deformation filed of the collagen substrate in 6 hours, with 10mins interval. Evolution of the gap size (c) and spatial distribution of the centripetal velocity (d). Data are presented as mean \pm s.e.m. n > 500 data points. Scale bar = 200 μ m.

Human tissues and organs have complex and varied shapes, and the deformation of cell populations in response to different geometric boundaries remains an important area of investigation^[29, 30]. To explore this relationship, we altered the shape of cell populations by

using PDMS masks to create straight or concave curved boundaries. We measured the velocity component of cells along the normal direction of the boundary to characterize their collective motion relative to the central positions, with positive values indicating contraction and negative values indicating expansion.

Cells exhibit random migration on solid substrates, and the boundary shifts to the cell-free area as the gap size decreases. However, when seeded on top of collagen, the cell population contracts, and the gap size increases within 6 hours (Fig.2c). The cell populations also undergo a transition from spreading to aggregating. Analysis of the average collagen deformation amplitude fields shows that a constant force field coupling between the cells population was approximately perpendicular to the boundary. Therefore, when the boundary curvature ≥ 0 , the coupling force fields point towards the interior of the cell population along the normal direction of the boundary.

We constructed a hollow geometric structure to further investigate the collective behaviors of cell populations on collagen substrates at negative curvature boundaries. For solid substrates, we covered PDMS masks (~2000 um in size) on a Petri dish and seeded cells around them, then removed the PDMS masks to create a hollow structure. However, the PDMS masks would destroy the surface structure of collagen hydrogels. Instead, we injected a bubble with a diameter of about 1500 um onto the collagen substrate and added the cell suspension around it. After cells adhered to the collagen substrate, the bubble was removed.

We used time-lapse microscopy to track the trajectories of cells and calculate the size of the "Wound Area" over time. The coordinates of the entire cell population were converted into a polar coordinate system with the wound center as the origin, and the whole pattern was divided into 36 regions in a 10° interval. The cells closest to the center in each region together form the cell population boundary. We used the "Boundary" and "Polyarea" functions in the MATLAB toolbox to obtain the area of the region enclosed by the boundary. The wounds on collagen hydrogel shrink faster than those on solid substrates (Fig.3f).

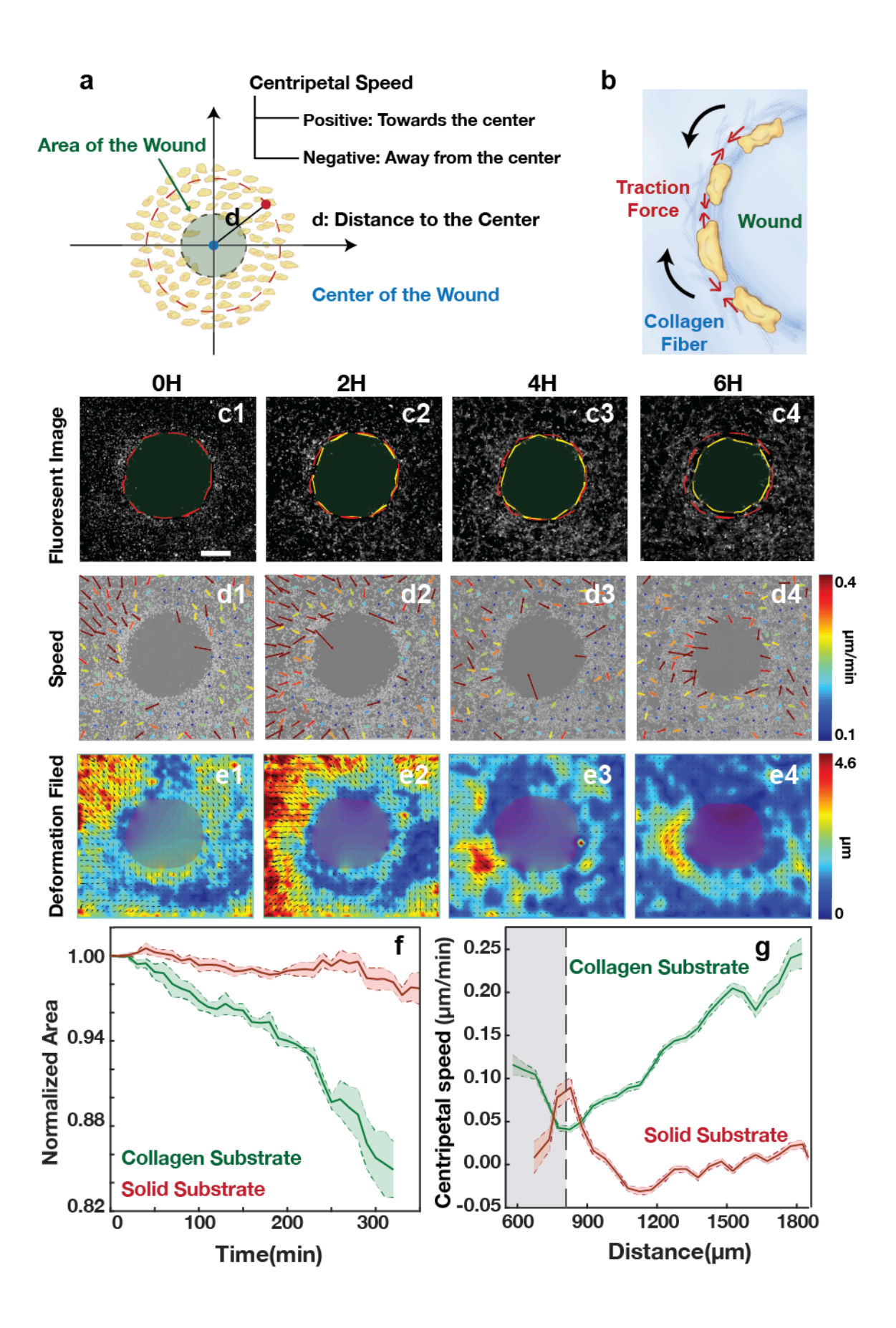


Figure3 Collective aggregation of cell population with "Wound Pattern". a) Schematic of the discrete cell population with a "Wound Pattern". b) Illustration of traction forces transited by collagen fiber bundles at the wound boundary. On the top of fibrous collagen hydrogel, the cell population aggregates toward the center and the wound decreases in size. Phase contrast images (c1-c4, red dashed line: wound boundary at 0H), cells velocity (d1-d4) and deformation filed with 10mins interval (e1-e4) for a "Wound Pattern" cell population with radius 1500 μ m on the collagen substrate. Evolution of the wound size (f) and spatial distribution of the centripetal velocity (g, gray area: cells near the boundary) on different substrates. Data are presented as mean \pm s.e.m. n > 500 data points. Scale bar = 400 μ m.

At the initial time point (0H), the traction forces of cells on the collagen substrate in the region far from the wound boundary are coupled to form a centripetal deformation field, with the deformation increasing with distance. However, the deformation field was in the centrifugal direction near the boundary. As the cell population shrinks, the direction of the deformation field near the wound boundary gradually changes to a centripetal direction (Fig. S3). To characterize the spatial distribution of cell motion, we calculated the centripetal velocity v and location d (distance to the wound center). The cell velocity distribution could be divided into two parts: 1) Far from the wound boundary (d > 825um, right side of the dotted line), the velocity was positively proportional to the distance, similar to the aggregation pattern of cells with a positive curvature boundary; 2) Near the wound boundary (d < 825um, left side of the dotted line), the centripetal velocity was inversely proportional to the distance (Fig.3g). The aggregation of cells near the wound boundary appeared to be due to the strong attraction between circumferentially adjacent cells, coupling into a centripetal force that resembled the effect of surface tension.

2.3 Re-Organized Fiber Bundle Network Regulates Collective Aggregation

Previous studies have shown that cells can re-organize collagen fibers to form thick fiber bundles parallel to the connecting cell centers. These re-organized fiber bundles transmit tension and induce strongly correlated migration of cells, which provides evidence for the collagen-matrix mediated attraction between cells^[25, 26]. To investigate the mechanism behind this strongly correlated aggregation behavior of MCF-10A cells on quasi-3D collagen hydrogel, we analyzed the collagen fibers around the cells using a laser scanning confocal microscope (SP8, Leica) in reflection mode.

Initially, collagen fibers are uniformly distributed on the substrate. However, as shown in Figure 4a-f, aggregated cells pull and reshape collagen fibers to form a network of fiber bundles. As cell aggregation occurs, the density distribution of collagen fiber networks tends to match the cell density distribution. For "Round Shape" cell populations, collagen density decreases from the center to the boundary, resulting in a radial fiber bundle network (Fig.4a-c, g-h). For "Wound Pattern" cell populations, collagen density decreases from the inner edge of the cell cluster to the periphery, and the shape of the fiber bundle at the wound boundary is circumferential, indicating the strong attraction between circumferential neighboring cells and confirming the ECM-mediated centripetal force field (Fig.4d-f, i-j). It

takes about 3 hours' evolution for the collagen fiber bundles with a circumferential structure to appear. This verifies that the circumferential attraction between cells gradually increases during the cells' migration, so the deformation field near the wound boundary changes from the centrifugal to the centripetal direction. The co-localization of cells with collagen fiber bundles during cell population evolution indicates that the ECM-mediated mechanical couplings between migrating cells lead to collective migration dynamics. To further verify this mechanism, we perform ECM-field coupled active-particle simulations which explicitly take into account the cell-ECM mechanical feedback mechanism. The numerical results are in excellent agreement with the experimental observation, further confirming the proposed coupling effects [SI- Section III].

Due to the remodeled microstructure of the collagen substrate, it no longer has uniform mechanical properties, and the deformation field of collagen cannot directly characterize the force field. To measure Young's modulus of collagen hydrogels with different microstructures, we used atomic force microscopy (AFM)^[31]. After three hours of cell population evolution on collagen substrates, the cell density distribution matches the collagen fiber bundle distribution. The high cell density corresponds to a high fiber concentration (Fig.4 i2-i3, j2-j3). We characterized the elastic modulus of collagen with different cell densities in "Wound Pattern" cell populations after 6 hours of evolution.

The AFM measurements were carried out in contact mode with F=10 nN (5~15 μ m indentation depths) and a constant loading speed v=10 μ m/s. The measured force–distance curves were recorded and fitted with Hertz model $F = \frac{4}{3(1-v^2)}ER^{0.5}\delta^{1.5}$ to calculate the

Young's modulus $E^{[32]}$, where F is the measured force, R is the probe radius, δ is the indentation distance, v is the Poisson ratio and v=0.49 $^{[33]}$. Fig.4l shows the force-indentation curves measured on the collagen gel at three different regions: no cell (black curve), low cell density (red curve), and high cell density (blue curve) (Fig. S4). The indentation force $F(\delta)$ is measured as a function of indentation δ when the AFM probe first moves downward against the collagen surface (approach, solid lines) and then moves backward away from the surface at the same speed (retract, doted lines). The yellow dashed lines show the fitting of the Hertz model to the approach curves. Fig.4m shows the variation of elastic modulus E in three different regions: no cell (21.72±4.50 Pa, N=21), low cell density (51.44±5.26 Pa, N=41), and high cell density (116.77±31.24 Pa, N=84). It indicates that, the region with dense collagen fiber bundle network has larger elastic modulus.

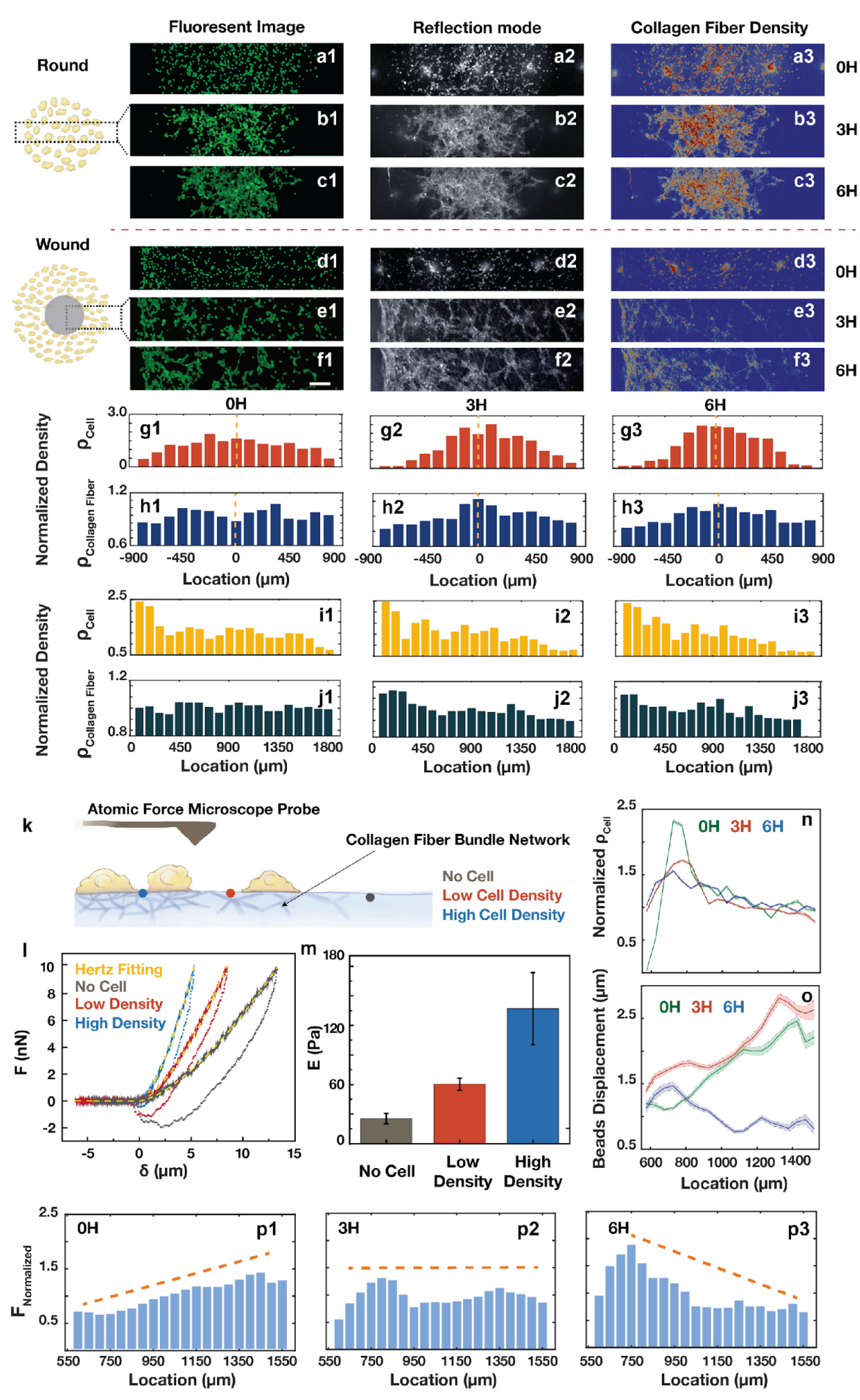


Figure 4 Re-Organized fiber bundle network induce cellular collective aggregation. a-c)

Fluorescent images (a1-c1), collagen fiber images recorded under the reflection mode (a2-c2) and map of collagen fiber density (a3-c3) for a selected area of the "Round Pattern" cell population (dashed box means the location of the selected area). Fluorescent images (d1-f1), collagen fiber images recorded in reflection mode (d2-f2) and map of collagen fiber density (d3-f3) for a selected area of the "Wound Pattern" cell population (dashed box means the location of the selected area) (Scale bar = 200 μm). g-j) The evolution of the spatial distributions of cells' density and collagen fiber in "Round Pattern" (g-h) and "Wound Pattern" cell population(i-j). k) Schematic of the mechanical measurement using AFM. I) Force-indentation curves measured on the collagen gel at three different regions: no cell (black curve), low cell density (red curve), and high cell density (blue curve). The indentation force $F(\delta)$ is measured as a function of indentation δ when the AFM probe first moves downward against the collagen surface at a constant loading speed v=10 μm/s (approach, solid lines) and then moves backward away from the surface at the same speed (retract, doted lines). The green dashed lines show the fitting of the Hertz model to the approach curves with E =21.04 Pa (no cell), 50.03 Pa (low cell density) and 103.85 Pa (high cell density). m) Variations of elastic modulus E in three different regions: no cell (25.48±5.29 Pa, N=21), low cell density (60.35±6.18 Pa, N=41), and high cell density (136.98 \pm 36.64 Pa, N=84). Data are presented as mean \pm s.d. The distributions of normalized cells' density (n), fluorescent beads' displacement (o), and the estimated traction force (p) at different time. Data are presented as mean \pm s.e.m.

We used the mechanical properties of re-shaped collagen and the deformation field to estimate the distribution of traction forces during the evolution of the "Wound Pattern" cell population. Initially, the collagen fibers were uniformly distributed, and the traction force was proportional to the displacement of the beads mixed in collagen. However, as the cell population evolved, the elastic modulus of the collagen became positively related to the density of the fiber bundles (which could be clarified by the cell density). Therefore, the distribution of the traction force field was estimated as the joint product of the normalized cell density and the displacement of beads (Fig.4p). As the "Wound Pattern" cell population evolved on the collagen substrate, along the radial direction, the distribution of the force field transitioned from decay to increase.

2.4 Effects of Collagen Microstructure and Universality of Cell-ECM Coupling Mechanism

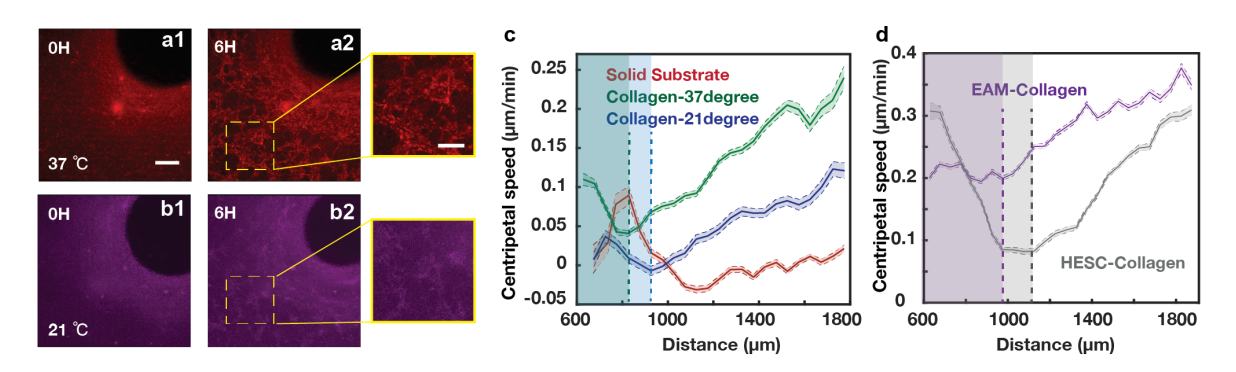


Figure 5 Cellular collective aggregation regulated by collagen microstructures and the collective migration of primary cell population. The evolution of the microstructure of the collagen fiber network re-organized by cells on the hydrogel with different gelation temperatures (a: 37°C, b: 21°C,

Scale bar = $200 \,\mu\text{m}$). An enlarged view of the collagen fiber network is represented in the yellow box (Scale bar = $100 \,\mu\text{m}$). c) Spatial distribution of the centripetal velocity of cells on different substrates (velocity of cells near the wound boundary are color labeled, green: 37°C , blue: 21°C). d) Spatial distribution of the centripetal velocity of primary cell population with "Wound Pattern" (velocity of cells near the wound boundary are color labeled, purple: EAM, gray: HESC).

The micromechanical properties of collagen gel are strongly influenced by its network architecture. The microstructure of collagen I can be modified by adjusting the gelation temperature, with higher temperatures resulting in a network composed of short and thin fibers, and lower temperatures leading to thicker fiber clusters^[34-36]. As a general trend, the heterogeneity of the network decreases as temperature increases. To investigate whether the microstructure of the extracellular matrix (ECM) can regulate the collective behavior of cells, we prepared a collagen I gel with a lower gelation temperature (21°C) to serve as a substrate for the "Wound Pattern" cell population.

We observed the cell population's evolution on the low gelation temperature collagen substrate and recorded the microstructure of the collagen fiber network using confocal microscopy. Compared to the high gelation temperature collagen (37°C), the cell population weakly re-organizes the fiber network as the gelation temperature decreases to 21°C. Even after 6 hours of evolution, the collagen with low gelation temperature does not form thick bundles, and the circular collagen fiber bundles at the wound boundary are not visible (Fig.5b, Fig. S5). The spatial distributions of cell motion on collagen substrate with different gelation temperatures follow a similar shape (Fig.5c). However, as the temperature decreases, the overall centripetal velocities of cells also decrease. Therefore, when the cells cannot effectively reconstruct collagen to apply attractive forces, the collective movement of the cells becomes weaker. The microstructure of the collagen gel can change the local mechanical properties and significantly affect the re-organization of fiber bundles, which in turn regulates the collective behavior of cells (Fig. S6).

To further verify the collagen-regulated collective organization behaviors, we tested different types of primary cells, including primary endometriosis-associated macrophages (EAM) and primary endometrial stromal cells (Human Endometrial Stromal Cells, HESC). When the cells were seeded as a "Wound Pattern", they also exhibited aggregative behaviors. Similar to the speed spatial distribution of MCF10A cells, those of the two types of primary cells can also be divided into two parts. The centripetal velocities of the peripheral cells positively relate to the distance. In contrast, for the cells closer to the boundary of the wound, centripetal velocities decrease with distance (Fig.5d). Thus, the previously proposed cell aggregation mechanism is universal: the interaction between the outer cells is enhanced due to the attractive force mediated by collagen fibers, resulting in a centripetal force field; while at the inner concave boundary, cells are continuously attracted towards the center due to the stronger circumferential attraction between the cells mediated by collagen fiber bundles.

3. Conclusion

We have demonstrated the significant role of cell-ECM mechanical coupling in regulating collective organizational behaviors of multi-cellular systems by unraveling a spreading-aggregating transition induced by collagen hydrogel. Our study reveals that with a "Round Pattern", the long-range mechanical coupling of individual migrating cells breaks the symmetry of random cellular motion and drives cell aggregation. In contrast, with a "Wound Pattern", strong contraction forces transmitted via fiber bundles between circumferentially adjacent cells cause collective centripetal migration near the concave boundary. Additionally, we demonstrate that fiber bundles formed due to the mechanical remodeling of the ECM by migrating cells can facilitate long-range force propagation in the ECM and regulate cell migration dynamics.

In epithelial monolayers or cell spheroids, intercellular adhesion, filamentous actin, and motor protein myosin II coordinate cell morphologies and collective migrations during tissue spreading and wound healing^[28, 37-41]. The ECM composition, viscosity, and rigidity regulate tissue spreading by affecting the orientation of actin stress fibers, cell migration mode, and cell-substrate interaction^[42]. An active aggregating-spreading transition in cells' monolayer is characterized by modifications in cell-cell adhesion, cell-substrate adhesion, cell contractility, and substrate stiffness, resulting in the competition between traction forces and contractile intercellular stresses^[43]. But in most experiments, the elastic modulus of soft polymer substrates is still higher than 1kPa, and the linear elastic materials, such as polyacrylamide gels, could not accurately mimic the structural remodeling and mechanics transmission of fibrous materials in vivo^[19, 21, 24, 37]. We emphasize that the strongly correlated long-range dynamic forces reported here, which govern the behavior of discrete cell populations, are transmitted through bundles of collagen fibers between individual cells rather than through intercellular adhesion as in previous studies on cell clusters.

Although recent research has highlighted the role of long-distance force in regulating tumor cell-immune cell interactions and collective invasion of cancer cells, the regulation of self-organization behaviors of population cells by intercellular mechanical signals remains poorly understood. To address this gap, we studied discrete cell populations in a quasi-3D model, which provided natural fiber hydrogels as a substrate to transmit force while avoiding the mechanical transfer generated by direct cell contact. Moreover, we quantified the correlation between cell dynamics, substrate deformation, and reshaped fiber bundle structure, providing direct experimental evidence for how the ECM mediates long-distance cell-cell interactions to regulate cell population behaviors. Our results provide new insights into regulating cell population behavior in tissue engineering, organ repair, and other important biological processes. By identifying the mechanisms underlying the spreading-aggregating transition in cell populations induced by collagen hydrogel, our study offers novel strategies for controlling cell population behavior in tissue engineering and regenerative medicine.

Acknowledgments

General: Thanks for the engineer of Soft Matter Lab Yongliang Zhai for the design and fabrication on the homemade live-cell incubating system.

Author Contributions:

Conceptualization: X.W., Q.F., Y.J. and F.Y.

Methodology: X.W., H.L., A.W.

Investigation: X.W., H.L., D.G., Q.F., Y.J. and F.Y.

Visualization: X.W., H.L.

Modeling and Simulation: Y.Z. and Y.J.

Writing—original draft: X.W., H.L., Q.F., Y.J. and F.Y.

Writing—review & editing: Q.F., Y.J. and F.Y.

Funding: This work was supported by The National Key Research and Development Program of China (Grant No. 2020YFA0908200, 2021YFA0719302), The National Natural Science Foundation of China (Grants No. 12074407, No.12090054, and No.11972351), the Strategic Priority Research Program of Chinese Academy of Sciences (Grant No. XDB33030300) and The Youth Innovation Promotion Association of CAS (no. 2021007).

Conflicts of Interest

The authors declare that they have no other competing interests.

Data Availability

All data needed in the paper are present in the paper and in the supplementary section. Additional data which are related to this paper may be requested from the authors.

Experimental Section

Cell Culture and Labeling:

The GFP-tagged normal human breast epithelial cell line MCF-10A cells (from the China Infrastructure of Cell Line Resource) were cultured in DMEM/F12 medium containing L-glutamine and 15mM HEPES (10-092-CVR, Corning), supplemented with 5% horse serum (16050-122, Gibco), 1% penicillin/streptomycin (30-002-CI, Corning), 20ng/mL human

epidermal growth factor (PHG0311, Gibco), 10µg/mL insulin (I-1882, Sigma), 100ng/mL cholera toxin (C-8052, Sigma) and 0.5 µg/mL hydrocortisone (H-0888, Sigma). The primary endometriosis-associated macrophages (EAM) and primary human endometrial stromal cells (HESC) were obtained from the lab of Prof. Ping Duan, the Second Affiliated Hospital of Wenzhou Medical University. EMAs and HESCs are extracted from the endometriosis tissue, including pelvic, peritoneal and other endometriosis lesions. EAMs were cultured in 1640 medium containing 10% FBS (Gibco) and 1% penicillin/streptomycin. HESCs were cultured in DMEM/F12 medium containing 10% FBS and 1% penicillin/streptomycin.

Cells were incubated at 37°C with 5% CO₂. Trypsin (25-053-CI, Corning) and 1 X PBS (46-013-CM, Corning) solution were applied to detach cells from the Petri dish. The cells were passaged every 5-6 days for a maximum of 20 passages. The primary cells were passaged for a maximum of 10 passages. We diluted 1µL Calcine AM (Invitrogen) into 1mL cell suspensions to fluorescently label primary cells. The cells were then incubated under the growth conditions for 30mins before a culture medium replaced the solution.

Collagen Gel Preparation:

Type I collagen extracted from rat tail tendon (Corning) was diluted into a final concentration of 2 mg/mL and neutralized pH to \approx 7 according to the product instructions. Collagen solution was added into a PDMS chamber (2mm height), attaching on the culture dish (Corning), and incubated at 37 °C for 30 min till gelation to form a collagen hydrogel substrate. For the quantitative characterization of the ECM deformation, fluorescent microbeads (Sphero) with a diameter of \approx 0.8 μ m were pre-mixed into the collagen solution, then uniformly embedded in the matrix as displacement markers after collagen gelation. The collagen solution was incubated at room temperature to get the collagen I gel with a lower gelation temperature.

Cell patterning on the solid or collagen substrate:

For the "Round Pattern" cell populations on a solid substrate, 300 cells were added in PDMS chambers (diameter of 2 mm), which were placed on the Petri dishes. One hour later, the cells attached to the substrate, and the PDMS chamber was removed. When the substrate was replaced by the collagen matrix, a 0.5µl drop containing approximately 300 cells was placed on top of the gels. After the cells were attached, the culture medium was added to cover the samples.

In the case of "Wound Pattern" cell populations on Petri dishes, the PDMS was cut into circles with a diameter of 2mm and pasted on the dishes. The cells were seeded around the PDMS with approximately $4*10^4$ cells/mL. For the cells on collagen, a bubble (with a diameter of about 1500 um) was injected onto the collagen substrate, and 5µl the cell suspension ($5*10^6$ cells/mL) was added around it. After cells adhered to the substrate, the PDMS mask or bubbles were removed, and more medium was added. The formation of the cell population's straight boundary was masked by a PDMS strip with a width of 2mm.

Imaging and cell tracking:

Inverted fluorescent microscopy (Nikon Ti-E) and confocal microscopy (Leica SP8) were used to acquire 2D and 3D time-lapse images (10X Air Objective lens). The microscopies worked with live-cell incubating systems, which could maintain the culture condition (37 $^{\circ}\mathrm{C}$, 5% CO2) for more than 24 hours. The time interval between the two scans was 10 mins. The reflection mode of the confocal microscopy was used to capture collagen-fiber microstructures (25X Water-immersion Objective Lens). The 3D multi-channel raw images were projected into 2D images with ImageJ (NIH). Software Imaris was used to track the time-dependent positions of the centroids of individual cells.

Analysis of ECM Deformation Fields:

The fluorescent beads mixed in the collagen hydrogel were dynamically tracked with the confocal microscope for 6 hours. The 3D images were projected into 2D images using ImageJ. The collagen ECM deformation fields were analyzed by PIV lab software based on the reference positions of the microbeads. Then the deformation parameters of the collagen matrix were quantitatively analyzed with MATLAB (MathWorks).

Analysis of cell density and collagen fiber density:

The confocal 3D reconstructed images were projected into 2D images using ImageJ. The gray value images were transferred into arrays. Along the x-axis, the images were separated into areas with a width of 400 pixels. The mean of gray value of each section was calculated to obtain a probability distribution of cells or collagen fibers.

AFM setup and operation:

Hydrogel force indentation measurements are performed using an AFM (MFP-3D, Asylum Research) with a colloidal probe. The AFM is set up on an inverted microscope (IX71, Olympus) equipped with an EMCCD camera (Ixon3, Andor). The colloidal probe consists of a glass sphere of radius R (≅25 μm), glued on the front end of a rectangular cantilever beam (NSC35/Pt, MikroMasch) featuring a spring constant of 11 N/m. The freshly assembled colloidal probe is plasma cleaned using a low-vacuum plasma cleaner (Harrick Plasma, PDC-32G) at the power of 40 W for 15 min. The vacuum level of the cleaner is kept at about 600 milli-torr during the plasma cleaning. The colloidal probe is then coated with a thin layer of poly(L-lysine)-graft-poly (ethylene glycol) (PLL-gPEG), which effectively reduces the adhesion of the hydrogel surface to the probe. Before each force measurement, the actual spring constant of the colloidal probe is calibrated in situ using the thermal power spectral density method. All experiments were carried out at room temperature. Each force indentation measurement was performed at least five times to ensure the reproducibility and accuracy of the experiment results.

The AFM measurements were carried out in contact mode with F=10 nN (5~15 μ m indentation depths) and a constant loading speed v=10 μ m/s. The measured force–distance curves were recorded and fitted with Hertz model $F=\frac{4}{3(1-v^2)}ER^{0.5}\delta^{1.5}$ to calculate the

Young's modulus E, where F is the measured force, R is the probe radius, δ is the indentation distance, v is the Poisson ratio and v=0.49.

References

- [1] P. Friedl, D. Gilmour, *Nat Rev Mol Cell Biol* **2009**, 10, 445.
- [2] X. Trepat, E. Sahai, *Nature Physics* **2018**, 14, 671.
- [3] R. Basu, B. M. Whitlock, J. Husson, A. Le Floc'h, W. Jin, A. Oyler-Yaniv, F. Dotiwala, G. Giannone, C. Hivroz, N. Biais, J. Lieberman, L. C. Kam, M. Huse, *Cell* **2016**, 165, 100.
- [4] R. Mayor, S. Etienne-Manneville, *Nat Rev Mol Cell Biol* **2016**, 17, 97.
- [5] I. Nitsan, S. Drori, Y. E. Lewis, S. Cohen, S. Tzlil, *Nature Physics* **2016**, 12, 472.
- [6] T. Zulueta-Coarasa, R. Fernandez-Gonzalez, *Nature Physics* **2018**, 14, 750.
- [7] X. Wang, S. Chen, H. Nan, R. Liu, Y. Ding, K. Song, J. Shuai, Q. Fan, Y. Zheng, F. Ye, Y. Jiao, L. Liu, *Research* 2021.
- [8] B. Ladoux, R. M. Mege, *Nat Rev Mol Cell Biol* **2017**, 18, 743.
- [9] A. Saraswathibhatla, D. Indana, O. Chaudhuri, *Nature Reviews Molecular Cell Biology* **2023**, DOI: 10.1038/s41580-023-00583-1.
- [10] O. Chaudhuri, J. Cooper-White, P. A. Janmey, D. J. Mooney, V. B. Shenoy, *Nature* **2020**, 584, 535.
- [11] O. Chaudhuri, S. T. Koshy, C. Branco da Cunha, J.-W. Shin, C. S. Verbeke, K. H. Allison, D. J. Mooney, *Nature Materials* **2014**, 13, 970.
- [12] X.-B. Zhao, Y.-P. Chen, M. Tan, L. Zhao, Y.-Y. Zhai, Y.-L. Sun, Y. Gong, X.-Q. Feng, J. Du, Y.-B. Fan, *Advanced Healthcare Materials* **2021**, 10, 2100821.
- [13] A. D. Doyle, N. Carvajal, A. Jin, K. Matsumoto, K. M. Yamada, *Nature Communications* **2015**, 6, 8720.
- [14] O. Chaudhuri, L. Gu, D. Klumpers, M. Darnell, S. A. Bencherif, J. C. Weaver, N. Huebsch, H.-p. Lee, E. Lippens, G. N. Duda, D. J. Mooney, *Nature Materials* **2016**, 15, 326.
- [15] M. Gómez-González, E. Latorre, M. Arroyo, X. Trepat, *Nature Reviews Physics* **2020**, 2, 300.
- [16] A. G. Clark, A. Maitra, C. Jacques, M. Bergert, C. Pérez-González, A. Simon, L. Lederer, A. Diz-Muñoz, X. Trepat, R. Voituriez, D. M. Vignjevic, *Nature Materials* **2022**, 21, 1200.
- [17] K. M. Yamada, M. Sixt, Nature Reviews Molecular Cell Biology 2019, 20, 738.
- [18] J. S. Di Martino, A. R. Nobre, C. Mondal, I. Taha, E. F. Farias, E. J. Fertig, A. Naba, J. A. Aguirre-Ghiso, J. J. Bravo-Cordero, *Nature Cancer* **2022**, 3, 90.
- [19] M. S. Hall, F. Alisafaei, E. Ban, X. Feng, C.-Y. Hui, V. B. Shenoy, M. Wu, *Proceedings of the National Academy of Sciences* **2016**, 113, 14043.
- [20] Y. L. Han, P. Ronceray, G. Xu, A. Malandrino, R. D. Kamm, M. Lenz, C. P. Broedersz, M. Guo, *Proceedings of the National Academy of Sciences* **2018**, 115, 4075.
- [21] J. P. Winer, S. Oake, P. A. Janmey, *PLoS One* **2009**, 4, e6382.
- [22] P. Ronceray, C. P. Broedersz, M. Lenz, *Proc Natl Acad Sci U S A* **2016**, 113, 2827.
- [23] Y. Zheng, Q. Fan, C. Z. Eddy, X. Wang, B. Sun, F. Ye, Y. Jiao, *Physical Review E* **2020**, 102, 052409.
- [24] R. S. Sopher, H. Tokash, S. Natan, M. Sharabi, O. Shelah, O. Tchaicheeyan, A. Lesman, *Biophysical Journal* **2018**, 115, 1357.

- [25] Q. Fan, Y. Zheng, X. Wang, R. Xie, Y. Ding, B. Wang, X. Yu, Y. Lu, L. Liu, Y. Li, M. Li, Y. Zhao, Y. Jiao, F. Ye, *Angewandte Chemie International Edition* **2021**, 60, 11858.
- [26] C. Yang, X. Wang, R. Xie, Y. Zhang, T. Xia, Y. Lu, F. Ye, P. Zhang, T. Cao, Y. Xu, Q. Fan, *Advanced Functional Materials* **2023**, 33, 2211807.
- [27] Y. Zheng, H. Nan, Y. Liu, Q. Fan, X. Wang, R. Liu, L. Liu, F. Ye, B. Sun, Y. Jiao, *Physical Review E* **2019**, 100, 043303.
- [28] C. P. Heisenberg, Y. Bellaiche, *Cell* **2013**, 153, 948.
- [29] T. Chen, A. Callan-Jones, E. Fedorov, A. Ravasio, A. Brugués, H. T. Ong, Y. Toyama, B. C. Low, X. Trepat, T. Shemesh, R. Voituriez, B. Ladoux, *Nature Physics* **2019**, 15, 393.
- [30] J. James, E. D. Goluch, H. Hu, C. Liu, M. Mrksich, Cell Motility 2008, 65, 841.
- [31] D. Guan, Y. Shen, R. Zhang, P. Huang, P.-Y. Lai, P. Tong, *Physical Review Research* **2021**, 3, 043166.
- [32] Hertz, Crelle's Journal 92, 156.
- [33] A. P. G. Castro, P. Laity, M. Shariatzadeh, C. Wittkowske, C. Holland, D. Lacroix, *Journal of Materials Science: Materials in Medicine* **2016**, 27, 79.
- [34] J. Xie, M. Bao, S. M. C. Bruekers, W. T. S. Huck, ACS Applied Materials & Interfaces 2017, 9, 19630.
- [35] C. A. R. Jones, L. Liang, D. Lin, Y. Jiao, B. Sun, Soft Matter 2014, 10, 8855.
- [36] C. A. R. Jones, M. Cibula, J. Feng, E. A. Krnacik, D. H. McIntyre, H. Levine, B. Sun, *Proceedings of the National Academy of Sciences* **2015**, 112, E5117.
- [37] G. Beaune, C. Blanch-Mercader, S. Douezan, J. Dumond, D. Gonzalez-Rodriguez, D. Cuvelier, T. Ondarçuhu, P. Sens, S. Dufour, M. P. Murrell, F. Brochard-Wyart, *Proceedings of the National Academy of Sciences* **2018**, 115, 12926.
- [38] G. Beaune, G. Duclos, N. Khalifat, T. V. Stirbat, D. M. Vignjevic, F. Brochard-Wyart, *Soft Matter* **2017**, 13, 8474.
- [39] S.-Z. Lin, B. Li, G.-K. Xu, X.-Q. Feng, Journal of Biomechanics 2017, 52, 140.
- [40] X. Wang, X. Xing, S. Lu, G. Du, Y. Zhang, Y. Ren, Y. Sun, J. Sun, Q. Fan, K. Liu, F. Wang, F. Ye, *Fundamental Research* **2022**, DOI: https://doi.org/10.1016/j.fmre.2022.01.031.
- [41] M. F. Staddon, M. P. Murrell, S. Banerjee, *Soft Matter* **2022**, 18, 7877.
- [42] S. Douezan, J. Dumond, F. Brochard-Wyart, Soft Matter 2012, 8, 4578.
- [43] C. Pérez-González, R. Alert, C. Blanch-Mercader, M. Gómez-González, T. Kolodziej, E. Bazellieres, J. Casademunt, X. Trepat, *Nature Physics* **2018**, 15, 79.